

## **Article 25fa pilot End User Agreement**

This publication is distributed under the terms of Article 25fa of the Dutch Copyright Act (Auteurswet) with explicit consent by the author. Dutch law entitles the maker of a short scientific work funded either wholly or partially by Dutch public funds to make that work publicly available for no consideration following a reasonable period of time after the work was first published, provided that clear reference is made to the source of the first publication of the work.

This publication is distributed under The Association of Universities in the Netherlands (VSNU) 'Article 25fa implementation' pilot project. In this pilot research outputs of researchers employed by Dutch Universities that comply with the legal requirements of Article 25fa of the Dutch Copyright Act are distributed online and free of cost or other barriers in institutional repositories. Research outputs are distributed six months after their first online publication in the original published version and with proper attribution to the source of the original publication.

You are permitted to download and use the publication for personal purposes. All rights remain with the author(s) and/or copyrights owner(s) of this work. Any use of the publication other than authorised under this licence or copyright law is prohibited.

If you believe that digital publication of certain material infringes any of your rights or (privacy) interests, please let the Library know, stating your reasons. In case of a legitimate complaint, the Library will make the material inaccessible and/or remove it from the website. Please contact the Library through email: [copyright@ubn.ru.nl](mailto:copyright@ubn.ru.nl), or send a letter to:

University Library  
Radboud University  
Copyright Information Point  
PO Box 9100  
6500 HA Nijmegen

You will be contacted as soon as possible.

# Noise Reduction in Computed Tomography Scans Using 3-D Anisotropic Hybrid Diffusion With Continuous Switch

Adriënné M. Mendrik\*, Evert-Jan Vonken, Annemarieke Rutten, Max A. Viergever, and Bram van Ginneken

**Abstract**—Noise filtering techniques that maintain image contrast while decreasing image noise have the potential to optimize the quality of computed tomography (CT) images acquired at reduced radiation dose. In this paper, a hybrid diffusion filter with continuous switch (HDCS) is introduced, which exploits the benefits of three-dimensional edge-enhancing diffusion (EED) and coherence-enhancing diffusion (CED). Noise is filtered, while edges, tubular structures, and small spherical structures are preserved. From ten high dose thorax CT scans, acquired at clinical doses, ultra low dose (15 mAs) scans were simulated and used to evaluate and compare HDCS to other diffusion filters, such as regularized Perona–Malik diffusion and EED. Quantitative results show that the HDCS filter outperforms the other filters in restoring the high dose CT scan from the corresponding simulated low dose scan. A qualitative evaluation was performed on filtered real low dose CT thorax scans. An expert observer scored artifacts as well as fine structures and was asked to choose one of three scans (two filtered (blinded), one unfiltered) for three different settings (trachea, lung, and mediastinal). Overall, the HDCS filtered scan was chosen most often.

**Index Terms**—Anisotropic diffusion, coherence-enhancing diffusion (CED), computed tomography (CT), edge-enhancing diffusion (EED), filter, noise reduction.

## I. INTRODUCTION

SINCE absorption of X-ray radiation increases the risk of inducing cancer to a patient, clinical research constantly aims at reducing the radiation dose [1]–[3]. One of the main drawbacks of decreasing the radiation dose is the increase in image noise. Kalra *et al.* [3] stated that further improvement of noise filtering techniques that maintain image contrast while decreasing image noise, is essential to optimize the quality of computed tomography (CT) images acquired at reduced radiation dose. Filtering noise from clinical scans is a challenging task, since these scans contain artifacts and consist of many structures with different shape, size, and contrast.

Manuscript received October 10, 2008; revised April 24, 2009. First published May 26, 2009; current version published September 25, 2009. *Asterisk indicates corresponding author.*

\*A. M. Mendrik is with the Image Sciences Institute, 3584 CX Utrecht, The Netherlands.

E.-J. Vonken and A. Rutten are with the Department of Radiology, University Medical Center Utrecht, 3508 Utrecht, The Netherlands.

M. A. Viergever and B. van Ginneken are with the Image Sciences Institute, 3584 CX Utrecht, The Netherlands.

Color versions of one or more of the figures in this paper are available online at <http://ieeexplore.ieee.org>.

Digital Object Identifier 10.1109/TMI.2009.2022368

Although prereconstruction noise filtering techniques perform especially well in suppressing structured noise in CT [4], raw scanner data is generally unavailable. Therefore, postreconstruction noise filtering techniques are usually used. Many of these noise filtering techniques are proposed in the literature [5], however diffusion filtering is often used in medical image processing. Meijering *et al.* [6] investigated the effect of applying edge-enhancing diffusion (EED) [7] and regularized Perona–Malik diffusion (RPM) [8] to three-dimensional rotational angiography (3DRA) scans. They found that EED performed better in smoothing the vessel wall, while RPM performed better in preserving local contrast in vessel segments with small diameters (less than three voxels). Their conclusion however was that as far as the trade-off between accuracy of quantification and quality of visualization was concerned, EED was to be preferred.

EED is one of two anisotropic diffusion filtering techniques introduced by Weickert [7]. The second is coherence-enhancing diffusion (CED). Three-dimensional EED preserves plate-like structures and filters noise from homogeneous areas, while CED filters tubular structures and preserves small spherical structures. Taking advantage of the properties of these anisotropic diffusion techniques, we propose to combine them by using a continuous switch, thus filtering noise while preserving as much structure as possible. Preliminary results on a smaller amount of data were published in [9]. Frangakis [10] and Fernandez [11] proposed to combine EED and CED using a discrete switch. As will be discussed, this switch lacks the ability to apply EED and CED appropriately in CT scans.

In this paper, the hybrid diffusion filter with continuous switch (HDCS) is presented and compared to several other diffusion filtering techniques. Background material and competing techniques are described in Section II. Section III describes how the HDCS filter exploits the properties of three-dimensional EED and CED, by a continuous combination of these filtering techniques. The qualitative and quantitative results of applying the filters to an artificial tube image, and clinical CT scans are shown in Section IV. In Section V these results are discussed and conclusions are drawn in Section VI.

## II. DIFFUSION FILTERING

Diffusion filtering of images is analogous to the physical diffusion process that equilibrates concentration differences without creating or destroying mass. In the last few decades, diffusion filtering has progressed from Gaussian smoothing [12]

to anisotropic nonlinear diffusion filtering [7]. The anisotropic diffusion equation is

$$\frac{\delta u}{\delta t} = \nabla \cdot (D \cdot \nabla u) \quad (1)$$

where  $\nabla \cdot$  is the divergence operator,  $\nabla u$  is the gradient of the image  $u$  and  $D$  is the diffusion tensor, which steers the diffusion. If the diffusion tensor  $D$  is replaced by a scalar-valued diffusivity  $g$ , the diffusion will be isotropic. The result  $\delta u / \delta t$  is the rate of change in intensity value in image  $u$  ( $u = u(t, x, y, z)$ ) at diffusion time  $t$ .

The most well-known form of diffusion filtering is homogeneous isotropic linear diffusion, more commonly known as Gaussian smoothing (GS). In this case the scalar-valued diffusivity  $g$  is set to 1. The resulting image  $u$  at diffusion time  $t$  can be obtained by convolving the original image  $f$  using a Gaussian kernel with standard deviation  $\sigma = \sqrt{2t}$ . This results in isotropic diffusion (equal smoothing in all directions) at every position in the image. Since there is no dependence on image structure, noise as well as structures are smoothed.

A way to adjust the diffusion process using image structure is to make the scalar-valued diffusivity  $g$  gradient dependent. Perona and Malik [13] introduced the nonlinear isotropic diffusion filter (terminology according to [7], [14]) with a rapidly decreasing diffusivity  $g$ . This filter was altered by Catte *et al.* [8] to regularized RPM. The diffusivity  $g$ , and therefore the size of the filtering kernel, depends on the local gradient magnitude squared  $g(|\nabla u_\sigma|^2)$ , causing the filter to be inhomogeneous. The scalar-valued diffusivity is defined as

$$g(|\nabla u_\sigma|^2) = 1 - e^{\frac{-C}{(|\nabla u_\sigma|^2 / \lambda^2)^4}} \quad (2)$$

where threshold parameter  $C = 3.31488$  as defined in [14], [15],  $\sigma$  is the scale at which the derivatives for the gradient ( $\nabla$ ) in image  $u$  are determined and  $\lambda$  is a contrast parameter, which determines whether the gradient magnitude indicates structure or noise. The diffusion process is still isotropic and almost no diffusion is performed when ( $|\nabla u_\sigma|^2 > \lambda^2$ ). Therefore edges are preserved, as well as noise near these edges.

Based on the anisotropic diffusion (1), Weickert introduced anisotropic diffusion filtering [14] (terminology according to [7] and [14]). Using the diffusion tensor to steer the filtering process allows for directional, anisotropic smoothing. The eigenvectors of the diffusion tensor define the principal directions of smoothing and the corresponding eigenvalues define the amount of smoothing. Weickert based the diffusion tensor on the structure tensor [7], [16], which describes structures in the image using first order derivative information. Therefore the principal directions of smoothing are based on the description of the structures. The structure tensor can be defined as [7]

$$J_\rho(\nabla u_\sigma) = K_\rho * (\nabla u_\sigma \nabla u_\sigma^T) \quad (3)$$

where  $K$  is the Gaussian kernel with standard deviation  $\rho$  (integration scale), over which the orientation information is averaged, and  $\nabla u_\sigma$  is the gradient of the image  $u$  at scale  $\sigma$ . Principle axis transformation gives the eigenvectors and eigenvalues of  $J_\rho(\nabla u_\sigma)$ .

Two specializations of anisotropic diffusion were introduced by Weickert, edge-enhancing diffusion (EED) and coherence-enhancing diffusion (CED) [14]. Both were initially defined in two dimensions. EED was designed to smooth noise while enhancing edges and CED was designed to enhance line-like textures. CED is essentially one dimensional diffusion [15], since there is either diffusion in one direction or almost no diffusion at all.

Since clinical scans are three dimensional, we are interested in the three-dimensional properties of EED and CED. EED in three dimensions becomes plate enhancing diffusion, it filters noise from homogeneous areas and enhances plate-like structures. If the eigenvalues of the structure tensor are set in order of decreasing magnitude ( $\mu_1 > \mu_2 > \mu_3$ ), the first eigenvector  $V_1$  of the structure tensor points in the direction of the highest gray level fluctuation. Therefore, in case of a plate-like structure,  $V_1$  points in the direction of the plate, while  $V_2$  and  $V_3$ , which are orthogonal to  $V_1$  and each other, run parallel to the plate. To be able to enhance the plate, strong diffusion is performed in the directions of  $V_2$  and  $V_3$ . Diffusion in the direction of  $V_1$  is set to be dependent on the gradient magnitude squared. Diffusion decreases if the gradient magnitude increases compared to the contrast parameter ( $\lambda_e$ ), indicating a plate-like structure. If the gradient magnitude is much smaller than  $\lambda_e$ , isotropic diffusion is performed. The eigenvalues of the 3-D EED diffusion tensor are defined as [6]

$$\begin{aligned} \lambda_{e1} &= \begin{cases} 1, & (|\nabla u_\sigma|^2 = 0) \\ 1 - e^{\frac{-C}{(|\nabla u_\sigma|^2 / \lambda_e^2)^4}}, & (|\nabla u_\sigma|^2 > 0) \end{cases} \\ \lambda_{e2} &= 1 \\ \lambda_{e3} &= 1 \end{aligned} \quad (4)$$

with a threshold parameter  $C = 3.31488$  as defined in [14] and [15].

As stated above, CED is essentially one dimensional diffusion. In 2-D images there is either diffusion in the direction of the eigenvector with the smallest eigenvalue ( $V_2$ ), or diffusion is minimized in both directions. Therefore three dimensional CED either performs diffusion in the direction of  $V_3$ , assuming that ( $\mu_1 > \mu_2 > \mu_3$ ) [15], or diffusion is minimized in all three directions. Accordingly, 3-D CED preserves small structures and enhances tubular structures. To decide whether diffusion should be performed, we use the ratio between the second and the third eigenvalue of the structure tensor. In tubular structures the ratio between these eigenvalues is large, while in small almost spherical structures the ratio is small. The eigenvalues of the 3-D CED diffusion tensor are defined as [15]

$$\begin{aligned} \lambda_{c1} &= \alpha \\ \lambda_{c2} &= \alpha \\ \lambda_{c3} &= \begin{cases} 1, & \text{if } \mu_2 = 0 \text{ or } \mu_3 = 0 \\ \alpha + (1 - \alpha) \cdot e^{\frac{-\ln(2) \cdot \lambda_c^2}{\kappa}}, & \text{otherwise} \end{cases} \end{aligned} \quad (5)$$

where  $\kappa = (\mu_2 / (\alpha + \mu_3))^4$ ,  $\alpha = 0.001$  [14] and  $\lambda_c$  is the CED contrast parameter. Setting  $\kappa$  to be the ratio between the second and third eigenvalue causes it to be independent of the contrast magnitude. Accordingly, if an image consists of tubes with different levels of contrast, all these tubes will be enhanced.

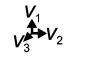
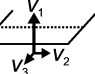
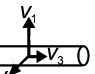
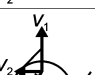

(a)		$\mu_1 \approx \mu_2 \approx \mu_3 \approx 0$	$\xi \approx 0$
(b)		$\mu_1 \gg \mu_2 \approx \mu_3$	$\xi \gg 0$
(c)		$\mu_1 \approx \mu_2 \gg \mu_3$	$\xi \ll 0$
(d)		$\mu_1 > \mu_2 > \mu_3$	$\xi < 0$
(e)		$\mu_1 \approx \mu_2 \approx \mu_3 \gg 0$	$\xi \approx 0$

Fig. 1. Illustration of the eigenvectors  $V_i$  (column 2) and corresponding eigenvalues  $\mu_i$  (column 3) of the structure tensor in five different situations. The last column illustrates the value of  $\xi$  defined in (7). (a) Almost no contrast in any direction, eigenvalues are equal and close to zero. (b) Contrast in the direction of  $V_1$ , first eigenvalue is much larger than the other two eigenvalues. (c) Contrast in the direction of  $V_1$  and  $V_2$ , first two eigenvalues are much larger than the third. (d) Much contrast in the direction of  $V_1$ , less contrast in the direction of  $V_2$ , and almost no contrast in the direction of  $V_3$ . First eigenvalue is larger than the second, which is larger than the third. (e) Contrast in all directions, eigenvalues are equal, but much larger than zero.

### III. HYBRID DIFFUSION WITH CONTINUOUS SWITCH

Medical images consist of many structures of different shape, size and contrast. If plain EED would be applied to medical images, it would filter noise and preserve plate-like structures, such as the boundaries of larger organs, but it would also blur vessels and smaller structures. Applying plain CED, on the other hand, would preserve smaller structures and filter vessels, but would not filter the noise and plate-like structures properly. Therefore to be able to exploit the properties of both EED and CED, it is necessary to combine them.

The diffusion tensors of EED and CED are both based on the structure tensor. Fig. 1 illustrates five situations, which could be encountered in medical images. The arrows indicate the eigenvectors ( $V_i$ ) of the structure tensor and the lengths of the arrows represent the magnitudes of the corresponding eigenvalues ( $\mu_i$ ). For filtering the situations in Fig. 1(a) and (b) EED should be used, while for filtering the situations in Fig. 1(c) and (e), CED is preferable. In the transitional phases between these situations [Fig. 1(d)], a combination of EED and CED can be used.

Frangakis and Hegerl [17] proposed to combine EED and CED by using a discrete switch based on the difference between the first ( $\mu_1$ ) and the third ( $\mu_3$ ) eigenvalue of the structure tensor and applied their filter to electron tomographic images. We will refer to this filter as HFH. Fig. 1(b) and (c) shows two different structures, a plate and a tube. In both cases, the difference between  $\mu_1$  and  $\mu_3$  is large. Therefore, using this difference as a discrete switch, will not lead to a distinction between situations in which EED should be applied and situations in which CED should be applied. Using the discrete switch, Fernandez and Li [11], [18] decided to adjust the definition of CED, such that it also filters plate-like structures. We will refer to this filter as HFL. Since EED already has the property of filtering plate-like

structures, using this discrete switch will not exploit the benefits of both EED and CED.

The limitation of using a discrete switch is that either EED or CED is used. In Fig. 1(d), however, a combination of EED and CED is preferred. To be able to deal with these intermediate geometries, we propose to combine EED and CED continuously, leading to hybrid diffusion with continuous switch (HDCS). The eigenvalues of the hybrid diffusion tensor ( $\lambda_{h_i}$ ) are set to be a linear combination of the eigenvalues of the EED ( $\lambda_{e_i}$ ) and CED ( $\lambda_{c_i}$ ) diffusion tensors

$$\lambda_{h_i} = (1 - \varepsilon) \cdot \lambda_{c_i} + \varepsilon \cdot \lambda_{e_i} \quad (6)$$

where the EED fraction ( $\varepsilon$ ) performs the switch between using the eigenvalues of the CED ( $\varepsilon \rightarrow 0$ ) or using the eigenvalues of the EED ( $\varepsilon \rightarrow 1$ ) diffusion tensor.

To distinguish between the various geometries depicted in Fig. 1(a)–(d), we propose to use the ratio between the various eigenvalues ( $\mu_i$ ) of the structure tensor as follows:

$$\xi = \left( \frac{\mu_1}{\alpha + \mu_2} - \frac{\mu_2}{\alpha + \mu_3} \right) \quad (7)$$

where  $\alpha = 0.001$  [14]. Fig. 1 illustrates that by using  $\xi$ , it is possible to distinguish between plate-like structures ( $\xi \gg 0$ ), tubular structures ( $\xi \ll 0$ ) and structures with similar eigenvalues in all directions ( $\xi \approx 0$ ).

For  $\xi \approx 0$  the eigenvalues of the structure tensor can be large, for small almost spherical structures, or small, for homogeneous areas (noise). In the former case, CED should be used to preserve small structures, while in the latter, EED should be used to filter noise isotropically. Therefore, when constructing the continuous switch using the ratio between the eigenvalues of the structure tensor ( $\xi$ ), a “small structure” correction ( $\mu_3/\lambda_h^2$ ) is incorporated into the switch. This enables it to distinguish between the two situations of equal eigenvalue-ratios. The contrast parameter  $\lambda_h$  is used to decide whether  $\mu_3$  indicates structure or noise. The final step in constructing a continuous switch between EED and CED, is incorporating a measure of magnitude. Although the eigenvalues of the structure tensor of noise in homogeneous areas are rather small, they can still differ an order of magnitude and produce eigenvalue ratios comparable to the ratios in Fig. 1(c). In this case, the ratio should not be taken into account, since EED should be used. Therefore a noise correction ( $\mu_2/\lambda_h^2$ ) is incorporated into the switch. The contrast parameter  $\lambda_h$  is again used to distinguish between structure and noise. The ratio between  $\mu_i$  is not taken into account if ( $\mu_2/\lambda_h^2$ ) indicates noise. This leads to the following definition of the EED fraction:

$$\begin{aligned} \varepsilon &= e^{\frac{\mu_2}{\lambda_h^2} \left( \frac{\xi - |\xi|}{2} - \frac{\mu_3}{\lambda_h^2} \right)} \\ &= e^{\frac{\mu_2 (\lambda_h^2 (\xi - |\xi|) - 2\mu_3)}{2\lambda_h^4}}. \end{aligned} \quad (8)$$

#### A. Parameter Settings

Because of discretization two extra parameters are introduced, time step size  $\tau$  and number of iterations  $\eta$ , which

TABLE I  
EVALUATED DIFFUSION FILTERS WITH THEIR PARAMETER SETTINGS USED FOR FILTERING PATIENT CT DATA. THE NUMBER OF ITERATIONS  $\eta$  WAS SELECTED TO HAVE THE SMALLEST RMS DIFFERENCE BETWEEN THE HIGH DOSE AND THE FILTERED SIMULATED LOW DOSE SCAN

Filter	Abbr.	Parameters
Gaussian Smoothing	GS	$\sigma = 1.0$
Regularized Perona-Malik Diffusion	RPM	$\sigma = 1.0, \lambda = 50.0, \tau = 0.11, \eta = 13$
Edge-Enhancing Diffusion	EED	$\sigma = 1.0, \lambda = 20.0, \tau = 0.11, \eta = 5$
Hybrid Diffusion Frangakis & Hegerl	HFH	$\sigma = 1.0, \lambda_e = 30.0, \lambda_c = 20.0, t_{ec} = 500.0$ $\rho = 1.0, \alpha = 0.001, \tau = 0.11, \eta = 15$
Hybrid Diffusion Fernandez & Li	HFL	$\sigma = 1.0, \lambda_e = 30.0, \lambda_c = 20.0, t_{ec} = 500.0$ $\rho = 1.0, \alpha = 0.001, \tau = 0.11, \eta = 7$
Hybrid Diffusion with Continuous Switch	HDCS	$\sigma = 1.0, \lambda_e = 30.0, \lambda_c = 15.0, \lambda_h = 30.0$ $\rho = 1.0, \alpha = 0.001, \tau = 0.11, \eta = 6$

together represent the diffusion time  $t$ . The explicitly discretized version of the anisotropic diffusion (1) is written as

$$u_i^{(\eta+1)\tau} = u_i^{\eta\tau} + \tau \cdot (\nabla \cdot (D \cdot \nabla u_i^{\eta\tau})) \quad (9)$$

where  $u_i^{(\eta+1)\tau}$  is the gray value of voxel  $i$  at time  $(\eta + 1)\tau$ . More about discretization schemes can be found in [19]–[21]. The time step size  $\tau$  is limited to

$$\tau \leq \frac{1}{2(1/s_x^2 + 1/s_y^2 + 1/s_z^2)} \quad (10)$$

where  $s_x, s_y, s_z$ , denote the voxel sizes in the  $x, y$ , and  $z$  direction, respectively [22]. The number of iterations ( $\eta$ ) times the time step size ( $\tau$ ) equals the diffusion time  $t$ . As the diffusion time increases, more noise will be filtered, but structure will eventually be lost. The number of iterations could be set by visually inspecting the resulting images, or by using one of the stopping criteria proposed in the literature [23].

The structure tensor and gradient magnitude are based on first order derivatives, which are determined at a certain scale ( $\sigma$ ). Increasing  $\sigma$  causes decreasing contrast at smaller structures, resulting in less small structure preservation. Decreasing  $\sigma$  however, causes the derivatives to be more sensitive to noise. For image restoration, typically in CT scans, a scale between 0.5 and 2.0 is suitable, depending on the amount of small structures and noise in the image.

The integration scale ( $\rho$ ) is used for the structure tensor and determines the area over which the neighboring first order derivatives (determined at scale  $\sigma$ ) are taken into account. The neighboring derivatives are taken into account such that at small interruptions in for example a line the diffusion takes place in the same direction as its neighbors, thus connecting the line. For restoration,  $\rho$  can be set between 0.5 and 2.0.

The hybrid contrast parameter ( $\lambda_h$ ) is used for the hybrid switch in (8). If  $\lambda_h$  is large, only high contrast small structures and tubes will be filtered with CED; EED will be used for the lower contrast small structures and tubes. If  $\lambda_h$  is too small, noise will be regarded as contrast and could be filtered using CED, which causes diffusion artifacts in noisy areas.

The EED contrast parameter ( $\lambda_e$ ) is used in (4). It indicates at which contrast the gradient magnitude represents an edge, instead of noise. It should be large enough to filter noise from the image, and small enough to preserve plate-like structures.

The CED contrast parameter ( $\lambda_c$ ) is used in (5). It indicates at which magnitude the ratio between the second and the third eigenvalue indicates a tubular structure. It should be small enough to filter tubular structures and large enough to preserve small spherical structures.

The regularization parameter ( $\alpha$ ) is used to make sure that the CED diffusion tensor matrix remains positive definite and is set to 0.001 [14]. It is also added to the eigenvalues of the structure tensor ( $\mu_i$ ), to prevent division by zero in (5) and (7).

When tuning parameters for filtering CT scans, the most important parameters to tune are  $\lambda_h, \lambda_e$  and the number of iterations ( $\eta$ ). For restoration purposes, the remaining parameters can be set as in Table I. Since  $\lambda_c$  acts as a counterbalance to the ratio between the second and third eigenvalue of the structure tensor, it has to be changed only if one wants the filtering in the direction of the third eigenvector to be performed at a smaller or larger ratio. For filtering CT scans  $\lambda_c$  can be set as in Table I. Fig. 2 illustrates the behavior of the HDCS filter for some choices of  $\lambda_h, \lambda_e$ , and  $\lambda_c$ . Table II gives the relation between the standard deviation within a region of interest (ROI) in a homogeneous area within the CT scan, with  $\lambda_h, \lambda_e$  and the number of iterations ( $\eta$ ). This table can be used as a guideline to set the HDCS parameters for CT scans. The standard deviation is measured in a ROI within the aorta.

#### IV. EVALUATION

For evaluation purposes, the HDCS filter and the diffusion filters described in Section II were applied to a 3-D artificial tube image as well as to patient CT scans. For the CT scans, which were acquired on a Philips Mx8000 IDT 16-slice CT scanner, both a quantitative and a qualitative evaluation were performed. The CED filter was excluded from the evaluation, because it was not designed to filter noise in homogeneous areas. The HFH and HFL filters are implemented using the EED and CED definitions defined in [11] and [17] and  $t_{ec}$  is the threshold value of the discrete switch [11].

##### A. Evaluation on an Artificial Tube Image

1) *Method*: An artificial tube image [Fig. 3(a)] was created, consisting of tubes with three different diameters (1, 2, and 4 pixels) at two intensities (20,  $-500$ ), while the background intensity is  $-1000$  (HU of air). Gaussian noise, with a mean of 0 and standard deviation of 100, was added [Fig. 3(b)]. The image

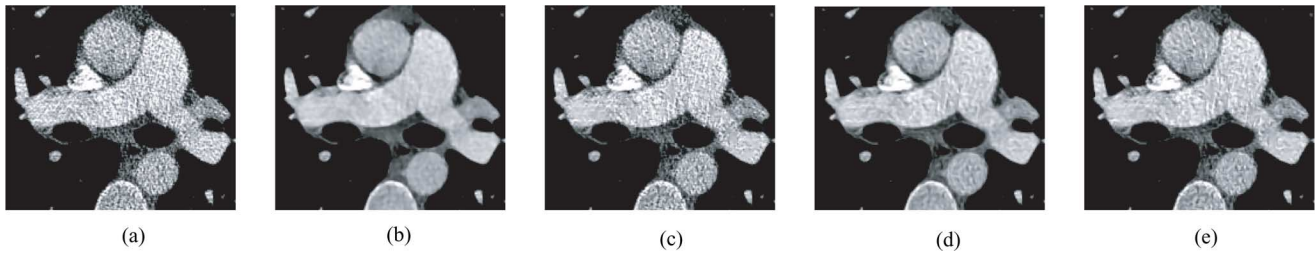


Fig. 2. Illustration of parameter settings. (a) Simulated low dose CT scan (segment of a slice: window = 550, level = 165). (b) Filtered with  $\lambda_h = 30, \lambda_e = 30, \lambda_c = 15$ . Optimal parameters for this scan. (c) Filtered with  $\lambda_h = 5, \lambda_e = 30, \lambda_c = 15$ . If  $\lambda_h$  is set too low, CED is used almost exclusively, which results in insufficient filtering of the noise in homogenous areas. (d) Filtered with  $\lambda_h = 30, \lambda_e = 5, \lambda_c = 15$ . If  $\lambda_e$  is set too low, some noise is interpreted as being edge, which results in smoothing in only two directions. (e) Filtered with  $\lambda_h = 5, \lambda_e = 30, \lambda_c = 1.0$ . If  $\lambda_h$  is set so low that CED is used almost exclusively, and  $\lambda_c$  is set so low that CED almost always smooths in the direction of the third eigenvector, the noise in homogeneous areas is structured in the direction of least contrast.

TABLE II  
PARAMETER SETTINGS FOR CT THORAX SCANS BASED ON THE STANDARD DEVIATION IN A REGION OF INTEREST WITHIN THE AORTA

std.dev	$\lambda_h/\lambda_e$	$\eta$
20-40	10	3
40-60	15	4
60-80	20	5
80-100	30	6

was filtered with the diffusion filters using 50 iterations for the iterative filters and Gaussian smoothing at scale 3.

2) *Results:* Fig. 3(c)–(h) shows the results of applying the diffusion filters.

### B. Quantitative Evaluation on CT Data

1) *Method:* For the quantitative evaluation, ten thorax CT scans were used acquired at clinical doses, with a tube current ranging from 130 to 284 mAs. For each of these scans an ultra low dose (15 mAs) scan was simulated using a model for adding physically realistic noise [24]. In this model, two images are reconstructed from the raw scanner data, the normal CT image and a pure noise image. Using these two images and assuming that the dominant part of the noise is X-ray photon noise, lower dose CT images are simulated by adding the simulated pure noise to the original data. Fig. 4 shows an example of the original high dose scan, the reconstructed pure noise image, and the corresponding simulated low dose scan.

Simulating low dose scans from the acquired high dose scans, rather than scanning the patient twice (high dose and low dose), reduces radiation dose and excludes registration errors. The simulated low dose scans were filtered using the filters and parameter settings listed in Table I. These parameter settings were determined in initial experiments by visually inspecting the results and quantitatively inspecting the difference to the high dose CT scan with various parameter settings. The time step size of the iterative filters depends on the voxel sizes of the CT data and was set to be below the value computed using (10).

From each of the ten patient CT scans four nonoverlapping, noncontiguous slabs of 25 slices were used for comparison, yielding 40 slabs (31 slabs containing predominantly lung parenchyma, six slabs containing mostly tissue, and three slabs with only tissue). For each high dose-filtered simulate low dose slab pair, the absolute mean difference was determined.

2) *Results:* Table III shows a ranking of the filters based on the root mean square (rms) of the absolute mean differences over all slab pairs. The HDSCS filter is ranked first place, with the smallest rms difference to the high dose scan. A paired two tailed T-test was performed and the results of the HDSCS filter were significantly different from the results of the other diffusion filters ( $P < 10^{-8}$ ). In Fig. 5, a maximum intensity projection slab of one of the patient thorax CT scans used in the quantitative evaluation is shown. When inspecting these images visually, the main areas of interest are the borders between various types of tissue, the preservation or enhancement of small structures (such as thin vessels in the lungs) and the noise filtered from the simulated low dose scan. Fig. 6 presents intensity profiles of a line through the maximum intensity projection slabs in Fig. 5, to illustrate the filtering properties of the various filters. The preservation of a small structure (calcified plaque) in the (filtered) low dose images is illustrated in Fig. 7.

### C. Qualitative Evaluation on CT Data

1) *Method:* Filtering simulated ultra low dose CT scans allows for quantitative evaluation, but the simulated data has limitations, for example electronic noise is not taken into account. Therefore the diffusion filters, using the parameter settings in Table I, were also applied to ten real low dose CT thorax scans, acquired with a tube current ranging from 34 to 60 mAs and a qualitative evaluation was performed. Of these scans, slabs were constructed showing three different settings: trachea, lung, and mediastinal. For the trachea setting, a coronal Minimum intensity projection (IP) of 6.3 mm was chosen at the level of the carina. For the lung setting, an axial Maximum IP of 6.3 mm was chosen at the level of the aortic arch. And for the mediastinal setting, an axial Average IP of 4.9 mm was chosen at the level of the heart. For the observer study, the original low dose slab and two filtered slabs were presented to an expert observer. The observer (blinded to the filter type used) was asked to rate fine structures (such as small vessels) and edges, and artifacts on a scale from 1 to 5 and to perform a forced choice test in which the observer had to choose which image was to be preferred: “No filtering,” “Filter 1,” or “Filter 2.” This test was performed 150 times, randomly varying filter pairs, clinical setting and patient scan. For the visibility of fine structures and edges, scores were assigned as follows: 1 (“excellent” visibility compared to low dose scan), 3 (no difference between low dose and filtered low



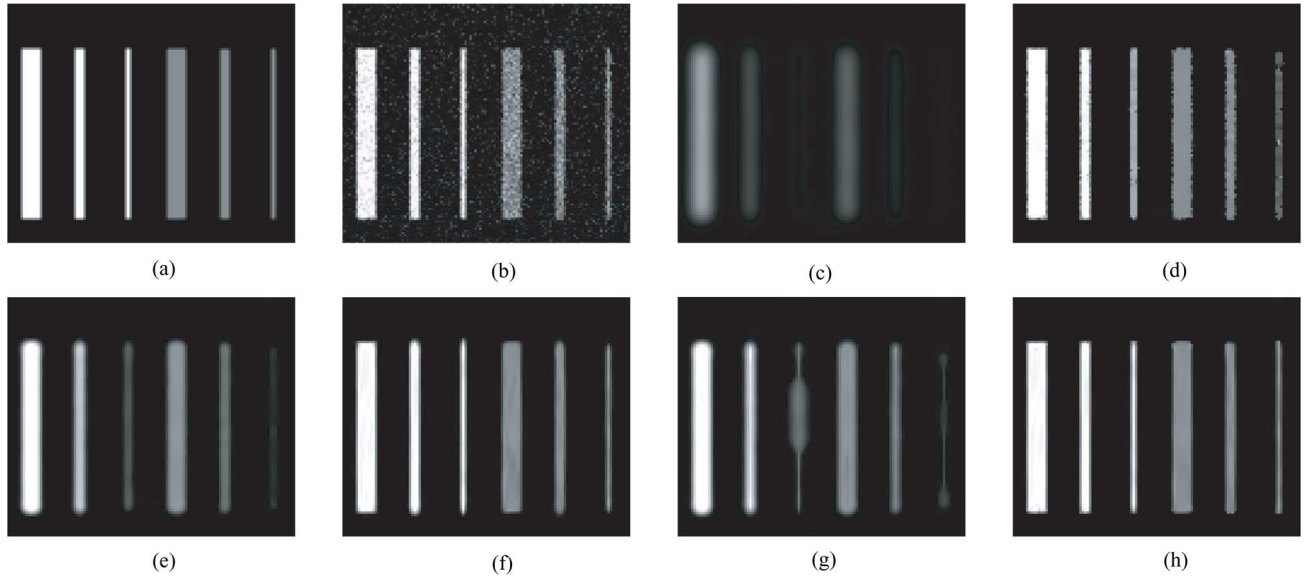


Fig. 3. One slice through the artificial tube image filtered with the various diffusion filters using 50 iterations for the iterative filters (window = 1020, level = -490). (a) Original image with tubes of different radius (1, 2, 4 pixels) and intensity (background = -1000, first 3 tubes = 20, last 3 tubes = -500). (b) Added Gaussian noise with mean 0.0 and std.dev. 100. (c) Gaussian smoothing with  $\sigma = 3.0$ . (d) Perona-Malik filtered with  $\sigma = 0.5$ ,  $\lambda = 60.0$ ,  $\tau = 0.15$ . (e) Edge-Enhancing Diffusion filtered with  $\sigma = 0.5$ ,  $\lambda = 10.0$ ,  $\tau = 0.15$ . (f) Filtered with hybrid diffusion of Frangakis and Hegerl with  $\sigma = 0.5$ ,  $\lambda_e = 50.0$ ,  $\lambda_c = 50.0$ ,  $t_{ec} = 500.0$ ,  $\rho = 1.0$ ,  $\alpha = 0.001$ ,  $\tau = 0.15$ . (g) Filtered with hybrid diffusion of Fernandez and Li with  $\sigma = 0.5$ ,  $\lambda_e = 50.0$ ,  $\lambda_c = 5.0$ ,  $t_{ec} = 500.0$ ,  $\rho = 1.0$ ,  $\alpha = 0.001$ ,  $\tau = 0.15$ . (h) Filtered with hybrid diffusion with continuous switch with  $\sigma = 0.5$ ,  $\lambda_e = 60.0$ ,  $\lambda_c = 20.0$ ,  $\lambda_h = 25.0$ ,  $\rho = 1.0$ ,  $\alpha = 0.001$ ,  $\tau = 0.15$ .

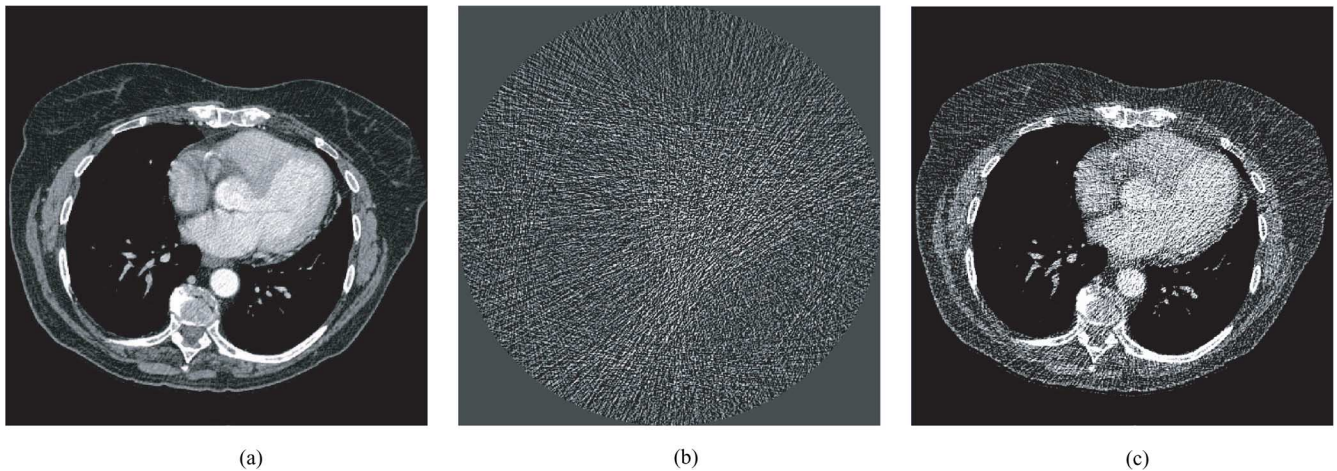


Fig. 4. Example of one of the high dose and simulated low dose patient thorax CT scans used for evaluating the HDCS filter. (a) shows an axial slice of the high dose CT scan acquired at 284 mAs (window = 400, level = 60), (b) shows the pure noise image (window = 70, level = 20) used for simulating the low dose scan, and (c) shows the corresponding axial slice of the simulated low dose (15 mAs) scan (window = 400, level = 60).

dose scan), and 5 (“very poor” visibility compared to low dose scan). Scores of 2 or 4 were assigned in between these extremes. The artifact scores were assigned as follows: 1 (improvement of CT artifacts), 2 (artifacts unaltered), 3 (slightly worsened), 4 (worsened), and 5 (severely worsened). If artifacts were worsened, this could be either because existing CT artifacts were enhanced or the noise filter introduced filtering artifacts.

2) *Results*: Table IV shows the results of the forced choice test. The observer chose “No filtering” in 8% of the mediastinal cases, in 17% of the trachea cases and in 55% of the lung cases. The results for the fine structure and artifact scoring are shown in Tables V and VI. In Fig. 8, an example of each setting (lung,

trachea, mediastinal) in the observer study is shown, as well as subimages of the real low dose filtered slabs.

## V. DISCUSSION

HDSCS was designed to filter noise in homogeneous areas and preserve structures of different shapes and sizes. Fig. 3 shows the results for an artificial tube image. Although this example concerns highly stylized images, it does illustrate the behavior of the diffusion filters. HDSCS is able to preserve the tubes, while filtering noise from the image. Real CT data, however, often contains structured noise (streak artifacts), which could be detected as tubes. Therefore the parameters have to be set such

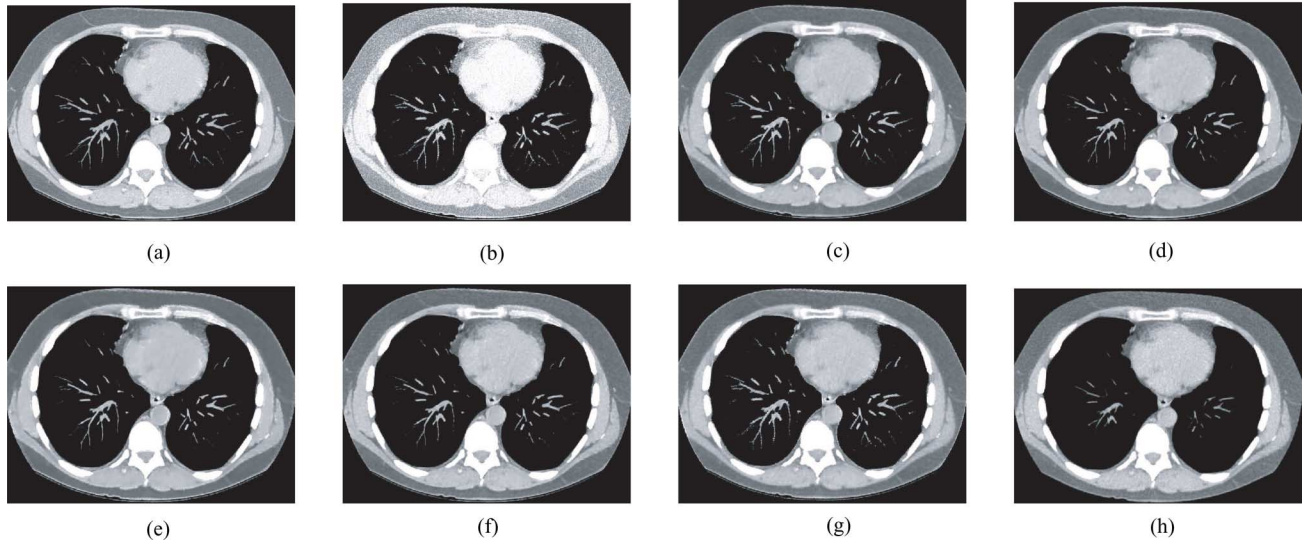


Fig. 5. Maximum intensity projection (MIP) slab (10.5 mm) of one of the patient thorax CT scans (window = 400, level = -50). The high dose scan was acquired at 215 mAs. The simulated low dose (15 mAs) CT scan was filtered using the filters and parameter settings listed in Table I, after which the MIPs were created. (a) High dose, (b) simulated low dose, (c) HDCS, (d) HFL, (e) HFH, (f) EED, (g) RPM, and (h) GS.

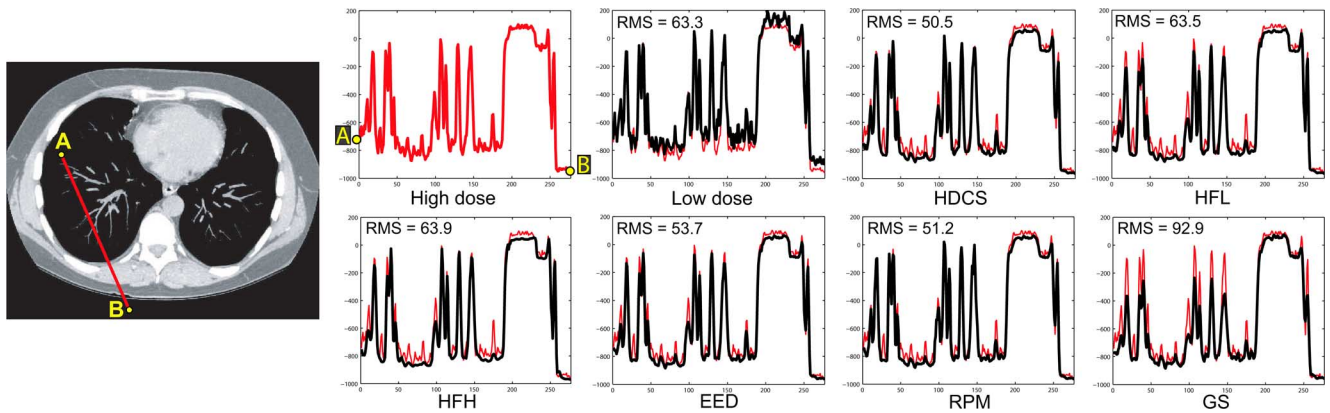


Fig. 6. Intensity profiles of a line on the maximum intensity projection slabs in Fig. 5, illustrating the filtering properties of the varying filters (parameter settings in Table I) on a simulated low dose CT thorax scan. In each filter plot, the high dose intensity profile is plotted in red and the rms difference to this high dose intensity profile is shown in the left top corner.

TABLE III  
RANKING OF THE FILTERS BASED ON THE RMS DIFFERENCE OVER 40 THORAX CT SCAN SLAB PAIRS (HIGH DOSE - (FILTERED) SIMULATED LOW DOSE). THE NUMBER OF ITERATIONS ( $\eta$ ) IS THE ONE GIVING THE LOWEST RMS DIFFERENCE

Rank	Filter	$\eta$	RMS diff.
1	HDCS filtered	6	17.94
2	HFL filtered	7	18.40
3	HFH filtered	15	18.59
4	EED filtered	5	18.63
5	RPM filtered	13	19.54
6	GS filtered	1	23.93
7	Unfiltered	-	43.22

that these artifacts are treated as noise, increasing  $\lambda_h$  and  $\lambda_e$ , which implies that structures with similar contrast will also be smoothed. This tradeoff between noise and contrast is an issue for all noise filters.

In Section IV-B, the results of the quantitative evaluation on CT scans were described and the filters were ranked according

to their rms difference. This ranking can be related to the properties of the filters. GS is ranked sixth, since both noise and edges are smoothed. RPM, ranked fifth, does preserve edges [Fig. 7(g)] while smoothing noise in homogeneous areas, but noise near edges is preserved as well [Fig. 3(d) and Fig. 5(g)]. EED and HFH are ranked fourth and third, respectively, their rms differences are similar. Unlike RPM, EED does smooth noise along the edge, but also smooths smaller structures, such as the thin tubes and calcified plaque in Fig. 3(e) and Fig. 7(f). HFH is able to preserve small structures [Fig. 3(f)], but introduces artifacts near edges [Fig. 5(e)]. These artifacts are caused by the CED filter which is applied near edges, due to the choice of the HFH discrete switch. Because of the artifacts near edges the HFH filter uses 15 iterations (similar to the RPM filter) to achieve the best rms difference, eventually blurring small vessels. HFL, ranked second, uses the HFH discrete switch, but due to the adjusted CED definition does not introduce edge artifacts, at the expense of small structure blurring [Fig. 7(d)] and introducing artifacts in small tubes [Fig. 3(g)]. However, only seven



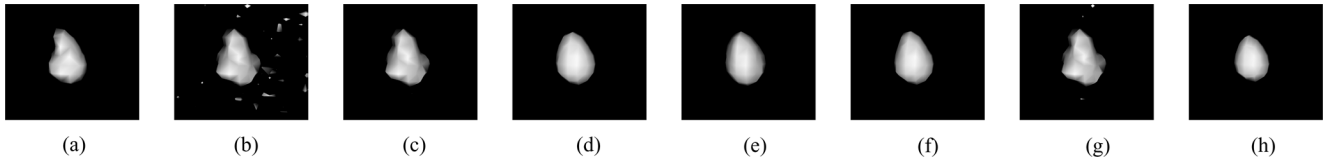


Fig. 7. Isosurface rendering of a calcified plaque, taken from a coronary artery in one of the thorax CT scans and filtered using the filters and parameter settings listed in Table I. The diameter of the calcified plaque on the high dose scan is approximately 1.7 mm (4 voxels). The isosurface threshold was set to 750 HU. (a) High dose, (b) Simulated low dose, (c) HDCS, (d) HFL, (e) HFH, (f) EED, (g) RPM, and (h) GS.

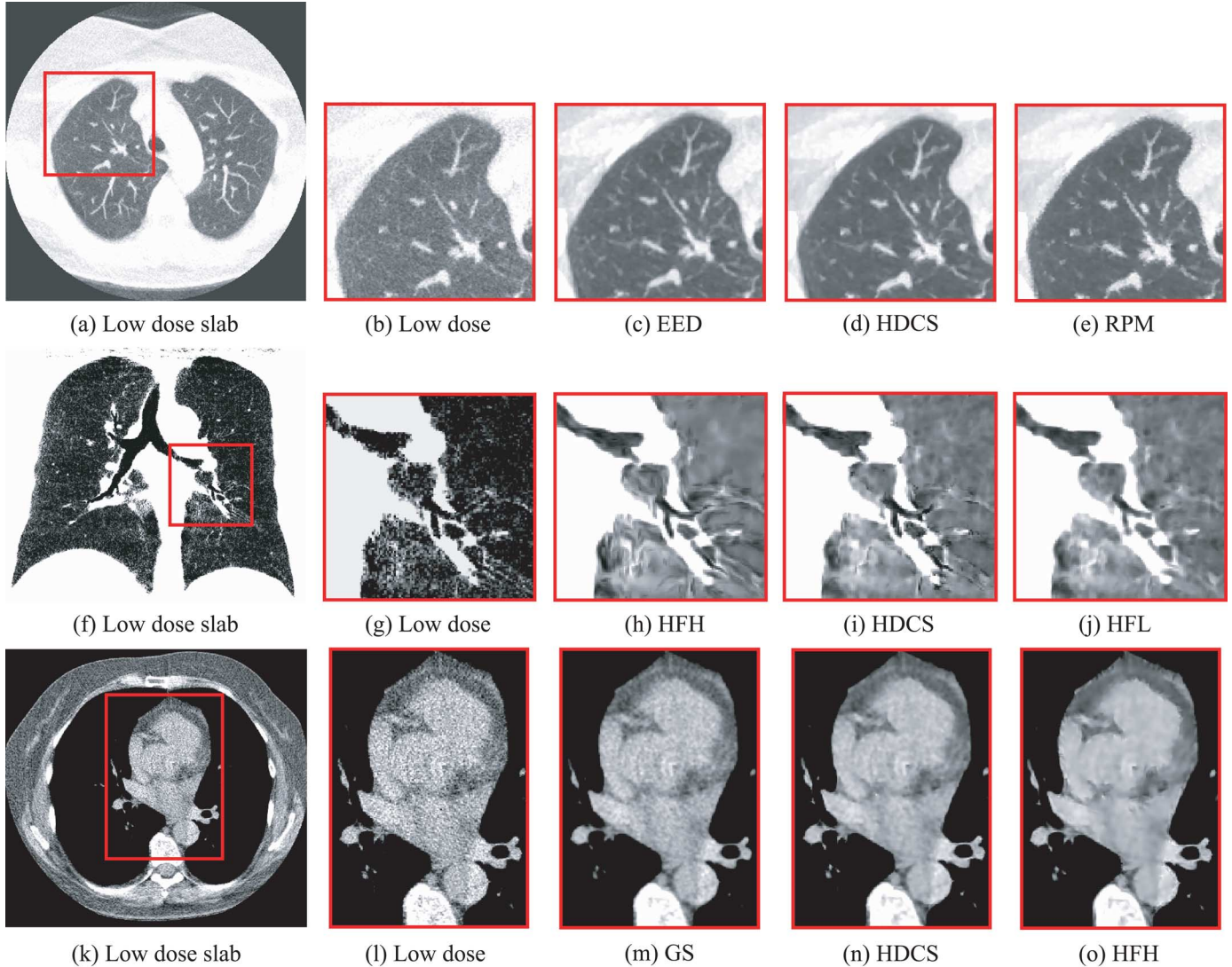


Fig. 8. Example of clinical settings in the observer study. (a) Lung setting (window = 1400, level = -600): Maximum Intensity Projection slab of 6.3 mm (Low dose scan 34 mAs). (f) Trachea setting (window = 300, level = -870): Minimum Intensity Projection slab of 6.3 mm (Low dose scan 35 mAs). (k) Mediastinal setting (window = 400, level = -50): Average Intensity slab of 4.9 mm (Low dose scan 34 mAs). (b,g,l) Low dose subimage. (c,h,m) Subimage of filtered slab chosen most often (see Table IV). (d,i,n) Subimage of HDCS filtered slab. (e,j,o) Subimage of filtered slab chosen least (see Table IV).

iterations are needed to achieve the best rms difference. HFL and HFH both use EED to filter small structures with equal contrast in all eigenvector directions. Therefore the calcified plaque in Fig. 7(d) and (e) is smoothed. HDCS is ranked first place and its rms difference is significantly different from the rms differences of the other evaluated diffusion filters. It uses 1 iteration more than EED and still results in a better preservation of small structures such as thin vessels [Fig. 5(c)] and calcified plaque [Fig. 7(c)]. This can also be seen from the intensity profiles in

Fig. 6, where HDCS shows to have the smallest rms difference to the high dose intensity profile. In this example RPM performs better than EED, since RPM results in a better small structure preservation, which has a large influence in this intensity profile. The rms differences of HFL and HFH are similar, since they both smooth the vessels (HFH because of the 15 iterations used). The example also illustrates that GS reduces contrast, since the GS intensity profile is almost completely located below the high dose profile.

TABLE IV

RESULTS OF THE BLINDED FORCED CHOICE TEST, IN WHICH THE OBSERVER HAD TO CHOOSE BETWEEN “FILTER 1,” “FILTER 2,” OR “NO FILTERING.” PERCENTAGES INDICATE IN HOW MANY PERCENT OF THE CASES A FILTER WAS CHOSEN TO PERFORM BEST

Setting	HDSCS	EED	HFH	HFL	RPM	GS
Lung	60%	100%	20%	60%	0%	50%
Trachea	68%	38%	100%	0%	13%	17%
Mediastinal	70%	56%	0%	44%	54%	100%
Overall	67%	61%	53%	31%	35%	60%

TABLE V

RESULTS OF THE ARTIFACT SCORING: THE PERCENTAGES INDICATE IN HOW MANY PERCENT OF THE CASES A CERTAIN SCORE (1 MUCH BETTER THAN LOW DOSE – 5 MUCH WORSE THAN LOW DOSE) WAS GIVEN

Score	HDSCS	EED	HFH	HFL	RPM	GS
1	57%	41%	34%	56%	57%	48%
2	35%	45%	45%	31%	29%	37%
3	5%	5%	16%	8%	6%	11%
4	3%	9%	5%	5%	9%	4%
5	0%	0%	0%	0%	0%	0%

TABLE VI

RESULTS OF THE FINE STRUCTURE AND EDGE SCORING: THE PERCENTAGES INDICATE IN HOW MANY PERCENT OF THE CASES A CERTAIN SCORE (1 EXCELLENT VISIBILITY – 5 VERY POOR VISIBILITY) WAS GIVEN

Score	HDSCS	EED	HFH	HFL	RPM	GS
1	0%	2%	2%	0%	0%	0%
2	28%	20%	35%	18%	6%	22%
3	55%	55%	15%	53%	60%	63%
4	15%	23%	44%	26%	31%	15%
5	1%	0%	5%	3%	3%	0%

The qualitative evaluation on real low dose CT thorax scans was described in Section IV-C. The results in Table IV show that the HDSCS filter was overall chosen most often by the observer (67%). Although other filters outperform the HDSCS filter in one clinical setting, they perform much worse in another clinical setting. The advantage of the HDSCS filter is that it performs equally well for all clinical settings (60%, 68%, 70%). This implies that it is the filter of choice when a more generally applicable filter is preferred. Why do the other filters perform so well in some settings and much worse in others? Although GS is the worst performing filter in the quantitative evaluation, in the forced choice test it was chosen most often (100%) in the mediastinal setting of the observer study. GS is applied with a  $\sigma$  of 1.0, which is sufficient for the mediastinum (Fig. 8), since it contains large structures of interest in which noise is smoothed and edge smoothing is minor. For the trachea setting on the other hand, GS is less suitable (17%), since it isotropically smooths the branches of the airway tree. In this setting HFH was chosen most often (100%). HFH uses CED in case of high contrast in the direction of the first eigenvector and low contrast in the direction of the third eigenvector, enhancing tube-like structures, such as the branches of the airway tree [Fig. 8(h)]. HDSCS [Fig. 8(i)] also uses CED to enhance tube-like structures, but since HFH uses 15 iterations versus 6 iterations of HDSCS, the branches of

the airway tree are enhanced more by HFH. In the mediastinal setting, however, HFH was chosen least (0%), due to the edge artifacts [Fig. 8(o)]. In the lung setting, EED was chosen most often (100%). Since EED uses one iteration less than HDSCS and the contrast parameter ( $\lambda$ ) is lower than with HDSCS (Table I), lower contrast structures in the lung parenchyma are smooth less [Fig. 8(c), (d)]. RPM was chosen least in the lung setting (0%). Presumably because the noisy edges make the image look artificial [Fig. 8(e)].

Instead of choosing one of the filters, the observer was also allowed to prefer no filtering above one of the filtered images in the forced choice test. The observer chose “no filtering” in 55% of all lung setting cases, whereas for the other two clinical settings this percentage was low. The reason for this is that the filter settings were too aggressive for this tissue type and removed fine details in the lung parenchyma. The results of scoring fine structures and artifacts were similar for the various filters. Table V shows that in general the CT artifacts were not worsened by the filters and Table VI shows that fine structures were, in most cases, similar to fine structures in the low dose scan. Only the results for the HFH filter were quite different from the other filters. This was due to the fact that it scored very well for the trachea setting, but very poorly for the mediastinal setting. The HDSCS filter scores well on both the artifact and fine structure scoring compared to the other filters.

A drawback of the HDSCS filter, is the number of parameters that has to be set. The guidelines in Section III-A give an insight into how these parameters influence the filtering process. As with most more advanced noise filters, the HDSCS filter has rather high demands in terms of computation time. Filtering a  $512 \times 512 \times 25$  image using 1 iteration, on an Intel Pentium 4 3.3 GHz with 2 Gb RAM, takes 40 s. The algorithm was implemented in C++ and not aggressively optimized for speed.

## VI. CONCLUSION

In this paper, we introduced the HDSCS filter and compared it to several existing diffusion filters. Quantitative experiments were performed on simulated low dose (15 mAs) patient thorax CT scans, which were compared to their corresponding high dose (range 130–284 mAs) scan. A qualitative evaluation was performed in the form of an observer study using real low dose CT data (range 34–60 mAs). We conclude that, based on the rms difference, the HDSCS filter performed best of all evaluated diffusion filters in reconstructing the high dose CT scans from their corresponding simulated low dose scans. According to the paired two tailed T-test, the results of the HDSCS filter were significantly different from the results of the other evaluated diffusion filters. Furthermore, the observer study showed that the HDSCS filter is generally applicable for multiple clinical settings.

## REFERENCES

- [1] A. B. De González and S. Darby, “Risk of cancer from diagnostic X-rays: Estimates for the UK and 14 other countries,” *Lancet*, vol. 363, no. 9406, pp. 345–351, 2004.
- [2] R. Doll and R. Peto, “The causes of cancer: Quantitative estimates of avoidable risks of cancer in the United States today,” *J. Nat. Cancer Inst.*, vol. 66, no. 6, pp. 1191–1308, 1981.
- [3] M. K. Kalra, M. M. Maher, T. L. Toth, L. M. Hamberg, M. A. Blake, J.-A. Shepard, and S. Saini, “Strategies for CT radiation dose optimization,” *Radiology*, vol. 230, no. 3, pp. 619–628, 2004.

- [4] M. Kachelriess, O. Watzke, and W. A. Kalender, "Generalized multi-dimensional adaptive filtering for conventional and spiral single-slice, multi-slice, and cone-beam CT.," *Med. Phys.*, vol. 28, no. 4, pp. 475–490, Apr. 2001.
- [5] A. Buades, B. Coll, and J. Morel, "A review of image denoising algorithms, with a new one," *Multiscale Model. Simul.*, vol. 4, no. 2, pp. 490–530, 2005.
- [6] E. Meijering, W. Niessen, and M. Viergever, "Diffusion-enhanced visualization and quantification of vascular anomalies in three-dimensional rotational angiography: Results of an in-vitro evaluation," *Med. Image Anal.*, vol. 6, no. 3, pp. 215–233, 2002.
- [7] J. Weickert, "A review of nonlinear diffusion filtering," in *Scale-Space Theory in Computer Vision*. New York: Springer, 1997, vol. 1252, Lecture Notes in Computer Science, pp. 3–28.
- [8] F. Catte, P.-L. Lions, J.-M. Morel, and T. Coll, "Image selective smoothing and edge detection by nonlinear diffusion," *SIAM J. Numer. Anal.*, vol. 29, no. 1, pp. 182–193, 1992.
- [9] A. Mendrik, E. Vonken, A. Schilham, M. Viergever, and B. Van Ginneken, "Hybrid diffusion compared with existing diffusion schemes on simulated low dose CT scans," in *Proc. Int. Symp. Biomed. Imag.*, Apr. 2006, pp. 1008–1011.
- [10] A. Frangakis and R. Hegerl, "Nonlinear anisotropic diffusion in three-dimensional electron microscopy," in *SCALE-SPACE'99: Proc. 2nd Int. Conf. Scale-Space Theories Comput. Vis.*, 1999, pp. 386–397.
- [11] J. Fernandez and S. Li, "An improved algorithm for anisotropic nonlinear diffusion for denoising cryo-tomograms," *J. Struct. Biol.*, vol. 144, pp. 152–161, 2003.
- [12] J. Koenderink, "The structure of images," *Biol. Cybern.*, vol. 50, pp. 363–370, 1984.
- [13] P. Perona and J. Malik, "Scale-space and edge detection using anisotropic diffusion," *IEEE Trans. Pattern Anal. Mach. Intell.*, vol. 12, no. 7, pp. 629–639, Jul. 1990.
- [14] J. Weickert, in *Anisotropic Diffusion in Image Processing*, B. G. Teubner, Ed., Stuttgart, Germany, 1998.
- [15] J. Weickert, "Coherence-enhancing diffusion filtering," *Int. J. Comput. Vis.*, vol. 31, no. 2–3, pp. 111–127, 1999.
- [16] R. San-Jose Estepar, "Local structure tensor for multidimensional signal processing. Applications to medical image analysis," Ph.D. dissertation, Univ. Valladolid, Valladolid, Spain, 2005.
- [17] A. Frangakis and R. Hegerl, "Noise reduction in electron tomographic reconstructions using nonlinear anisotropic diffusion," *J. Struct. Biol.*, vol. 135, pp. 239–250, 2001.
- [18] J. Fernandez and S. Li, "Anisotropic nonlinear filtering of cellular structures in cryoelectron tomography," *Comput. Sci. Eng.*, vol. 7, no. 5, pp. 54–61, 2005.
- [19] J. Weickert and H. Schar, "A scheme for coherence-enhancing diffusion filtering with optimized rotation invariance," *J. Vis. Commun. Image Represent.*, vol. 13, no. 1–2, pp. 103–118, 2002.
- [20] H. Schar and D. Uttenweiler, "3D anisotropic diffusion filtering for enhancing noisy actin filament fluorescence images," in *Proc. Pattern Recognition: 23rd DAGM Symp.*, Munich, Germany, Sep. 12–14, 2001, vol. 2191, pp. 69–75.
- [21] H. Spies and H. Schar, "Accurate optical flow in noisy image sequences," in *Proc. 8th Int. Conf. Comput. Vis. (ICCV'01)*, 2001, vol. 1, pp. 587–592.
- [22] W. Niessen, B. Ter Haar Romeny, L. Florack, and M. Viergever, "A general framework for geometry-driven evolution equations," *Int. J. Comput. Vis.*, vol. 21, pp. 187–205, 1997.
- [23] P. Mrazek and M. Navara, "Selection of optimal stopping time for nonlinear diffusion filtering," *Int. J. Comput. Vis.*, vol. 52, no. 2–3, pp. 189–203, 2003.
- [24] O. Amir, D. Braunstein, and A. Altman, "Dose optimization tool," *Med. Imag.*, vol. 5029, pp. 815–821, 2003.